# Combined Light Scattering and Laser Scanning Confocal Microscopy Studies of a Polymer Mixture Involving a Percolation-to-Cluster Transition

**Hiroyuki Takeno,† Mitsuhiro Iwata,‡ Mikihito Takenaka, and Takeji Hashimoto***

*Department of Polymer Chemistry, Graduate School of Engineering, Kyoto University, Kyoto 606-8501, Japan*

*Received July 25, 2000*

ABSTRACT: The time evolution of a phase-separated morphology in a binary polymer mixture involving a percolation-to-cluster transition (PCT) was investigated by a combined use of laser scanning confocal microscopy (LSCM) and light scattering (LS). We constructed *three-dimensional* images of phase-separating structures in the PCT process by means of the LSCM technique. The three-dimensional image observed by the LSCM was found to be consistent with the result from the LS, revealing that the phase separation process can be classified into four regimes: (i) percolation regime, (ii) PCT-I regime, (iii) PCT-II regime, and (iv) cluster regime. Details of phase separation dynamics in each regime are described in the text.

## I. Introduction

Many studies have been so far conducted on relationships between dynamics and morphological evolution of mixtures via spinodal decomposition (SD). The scattering technique such as light scattering (LS) and neutron scattering (NS) and real space observation such as transmission electron microscopy (TEM) and optical microscopy (OM) have been used to carry out such studies. Recently, laser scanning confocal microscopy (LSCM) attracts our attention as a very powerful technique to observe the three-dimensionally phase-separated morphology. The LSCM allows us to detect only the light reflected or emitted very close from a focal plane by excluding the light reflected or emitted from out of the focal plane by use of a "confocal pinhole", as detailed in the literature.[1] We can obtain three-dimensional information on the phase-separated structures from a series of sliced images obtained by moving the focal plane along the depth direction of the specimen (parallel to the incident beam axis). In fact, Jinnai et al. successfully constructed a three-dimensional image of the bicontinuous phase-separated structures by computationally stacking such images.[2] Moreover, they showed that the square of the magnitude of the Fourier transform of the three-dimensional image was consistent with the structure factor directly obtained from the LS experiment.[2−5]

On the other hand, in recent years some researchers have focused on studies of phase separation dynamics for systems undergoing the change in the phase-separating morphology from percolation structures to cluster of droplets {percolation-to-cluster transition (PCT)} by use of LS,[6−8] OM, TEM,[9−11] and computer simulation.[12−14] In some cases, it is difficult to judge whether the phase-separating domains observed by TEM or OM images are percolation structures or a cluster of droplets. If the focal depth is larger than size of the droplets densely packed in space, we may be misled to interpret the structure appeared on the image as percolating domains. Contrary to this, if the focal depth is much smaller than characteristic size (periodicity) of the percolating structures or if we observe an ultrathin section of the samples containing the percolating structures with its thickness much smaller than the characteristic size of the percolating structures, as is often the case with TEM observation, then we may mistake the percolating domains as a cluster of droplets. To circumvent such difficulties as described above, the LSCM can be used as a very useful method, because it enables us to have three-dimensional information on phase-separating structures.

In this study we attempted to use LSCM and LS in order to investigate the phase separation dynamics involving PCT for a mixture of poly(styrene-*ran*-butadiene) (SBR) and polybutadiene end-capped with fluorescein (PB-fl) (hereafter this mixture is denoted by SBR/PB-fl). Here we discuss the relationship between the phase-separating morphology as observed by LSCM and the phase separation kinetics as studied by LS.

## II. Experimental Section

**A. Sample Characteristics and Preparation.** The PB-fl and SBR used in this study have a weight-average molecular weight $M_w$ of $10.6 \times 10^4$ and $8.3 \times 10^4$, respectively, and a heterogeneity index for molecular weight distribution $M_w/M_n$ of 1.03 and 1.2, respectively, where $M_n$ is the number-average molecular weight. The PB-fl with 1,2 linkage content of 31% and 1,4 linkage content of 69% is terminated with fluorescein, which absorbs the light of wavelength of $\lambda = 480$ nm and emits the fluorescent light of $\lambda = 516$ nm. The fluorescein labeling is useful to clearly distinguish the PB-fl-rich phase from the SBR-rich phase in LSCM observation of phase-separating structures using an Ar ion laser with $\lambda = 488$ nm. The SBR contains 20% styrene. The butadiene part of SBR has 1,2 linkage content of 52%, 1,4-cis linkage content of 17%, and 1,4-trans linkage content of 31%. Note that the difference in fraction of 1,2-linkage between PB-fl and the butadiene part of SBR is due to a difference in the polymerization conditions used.

The mixture of SBR and PB-fl with a given composition was dissolved in toluene to make a solution containing 2 wt % polymers in total, and then the solution was filtered by using

† Current address: Department of Biological and Chemical Engineering, Faculty of Engineering, Gunma University, Kiryu, Gunma 376-8515, Japan.

‡ Current address: Research & Development Center, Yokohama Rubber Co. Ltd., Oiwake, Hiratsuka, Kanagawa 254-8601, Japan.

* To whom correspondence should be addressed.

10.1021/ma001316u CCC: $19.00 
Published on Web 11/30/2000

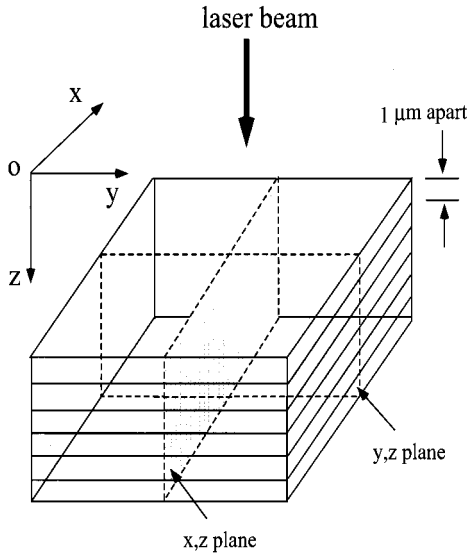


**Figure 1.** Schematic representation of the scanning geometry in the LSCM measurements. The incident laser beam travels along the *z*-direction. Three-dimensional images of the phase-separating domains are obtained by shifting the focal plane (*x*,*y*-plane) along the *z*-direction and computationally stacking the LSCM sliced images taken from the respective focal planes. A cross-sectional image of phase-separating domains in the *x*,*z*-plane and that in the *y*,*z*-plane are obtained by cutting the stacked images with each plane perpendicular to *y*- or *x*-axis, respectively.

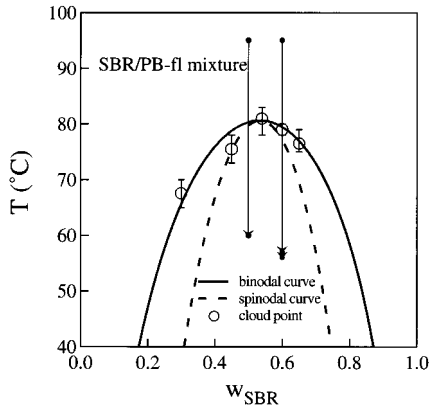


**Figure 2.** Cloud points, spinodal (dashed line) curves, and binodal curves (solid line) for the SBR/PB-fl mixtures.

a Millipore filter with a pore size of 0.45 $\mu$m to remove impurities. The filtered solution was cast on a Petri dish at ca. 20 °C. Film specimens of the SBR/PB-fl mixtures with compositions of 50/50 and 60/40 in weight percent were prepared by slowly evaporating solvent. As will be shown in Figure 2, this mixture has an upper critical solution temperature type phase diagram with a critical temperature of 81 °C. Therefore, the as-cast sample was phase-separated. We cannot immediately obtain the homogeneous sample, even if we bring the as-cast sample into the single-phase state by raising temperature, since dynamics of polymers with high molecular weight is very slow. Therefore, we homogenized the as-cast sample by mechanical mixing using Baker's transformation,[15] and afterward we annealed it for a few hours at 95 °C in the single-phase state. The sample obtained in this manner was transparent at 95 °C. We brought the sample into the two-phase state for isothermal phase separation experiments by rapidly lowering temperature.

**B. Laser Scanning Confocal Microscopy (LSCM).** LSCM measurements were performed with a Carl Zeiss LSM 320 using an Ar ion laser with wavelength of 488 nm as an incident beam which excites fluorescein. The fluorescent light emitted from PB-fl was passed through a narrow band path filter of 515−565 nm and detected with a photomultiplier. The measured fluorescence intensities were used to create images as will be detailed. The schematic diagram of the scanning geometry in the LSCM observations is shown in Figure 1. The incident laser beam propagates along the *z*-direction. In the LSCM method, we obtained a sliced image of structures on the focal plane (*x*,*y*-plane) at a given focal point, *z*, with a focal depth of ca. 0.9 $\mu$m. Then we shifted the focal depth along *z*-direction to take a series of sliced images (up to 30−50 images) at every 1 $\mu$m distance along *z*-direction. By using software incorporated with the LSCM apparatus, we obtained cross-sectional images parallel to the *x*,*z*-plane or to the *y*,*z*-plane by cutting the piled images with each plane at a given position along *y* and *x*, respectively, as shown in Figure 1. In some figures (Figures 5, 7, 8, and 10), we present the three orthogonal cross-sectional images (*y*,*z*-, *x*,*z*-, and *x*,*y*-section) at a given point (*x*, *y*, *z*) of the phase-separating structures. Furthermore, we computationally constructed a three-dimensional image of phase-separating domains based on the 30 LSCM slices piled in the above manner, according to the method described elsewhere.[2,16]

**C. Transmission Electron Microscopy (TEM).** At an early time of phase separation, phase-separating structures are so small that we cannot observe them by means of LSCM. In such instances, we used transmission electron microscopy (TEM) instead of LSCM. In TEM observation of the phase-separating structures at a given time after the onset of phase separation, the phase-separating sample was first quenched with liquid nitrogen in order to freeze growth of the phase-separating structure at that time. Then, the frozen sample was cut into ultrathin sections of ca. 50 nm thickness by using an ultramicrotome at ca. −120 °C, and the ultrathin sections were stained and fixed[17] with osmium tetraoxide ($OsO_4$) vapor. $OsO_4$ selectively reacts with butadiene monomer units in both PB-fl and SBR, giving a relatively darker contrast to the PB-rich phase than to the SBR-rich phase under TEM observation.

**D. Light Scattering (LS).** To investigate phase-separation dynamics, we carried out time-resolved LS measurements with a He−Ne laser of wavelength 632.8 nm. More specifically, we measured the time change in the LS profiles after temperature jump from a given temperature (95 °C) in the single-phase state into target temperatures in the two-phase state as shown by the arrows in Figure 2. We determined cloud points of the mixtures shown in Figure 2 (with open circles) by taking account of the fact that phase-separation kinetics are extremely slow near the binodal line for polymer mixtures with high molecular weight. We first compared the LS profile that was measured after annealing the mixture at a given temperature *T* for a few days with that measured at 95 °C in the single-phase state. If the LS profile measured at *T* has higher intensities than that at 95 °C, we assessed the mixture was in the two-phase state at that temperature *T*. Otherwise, we assessed the mixture was in the single-phase state at that temperature. By carrying out this kind of measurement at various temperatures and for various compositions, we obtained cloud points for the SBR/PB-fl mixtures.

## III. Results and Discussion

**A. Cloud Points.** In Figure 2 we show the result of cloud points determined by LS for the SBR/PB-fl mixtures. The mixtures have an upper critical solution temperature (UCST) type phase diagram: at temperatures above the cloud-point curve, the mixture is in the single-phase state, while at temperatures below, the mixture is in the two-phase state. We determined the binodal curve (shown by the solid line in Figure 2) by a best fit of the theoretical curve obtained on the basis of the Flory−Huggins theory to the cloud point data. Moreover, we calculated the spinodal curve (dotted line) by using the Flory−Huggins interaction parameter $\chi$ obtained in the fitting procedure described above. Details of the procedure were described elsewhere.[18]

**B. Time Evolution of $q_m$ and $I_m$.** In the phase separation experiment using the scattering technique, the time evolution of the phase-separating structure is characterized by the peak wave vector $q$ ($q_m$) at which the scattered intensity $I(q)$ is maximized to $I_m$ [$I_m \equiv I(q = q_m)$], where the wavenumber $q$ is defined as follows:

$$q = (4\pi/\lambda)\sin(\theta/2) \tag{1}$$

$\lambda$ and $\theta$ are wavelength and scattering angle in the sample, respectively. The $q_m$ and $I_m$ often obey the power law with time $t$:

$$q_m \sim t^{-\alpha} \tag{2}$$

and

$$I_m \sim t^{\beta} \tag{3}$$

The scaling exponents $\alpha$ and $\beta$ depend on the phase separation mechanism, and $q_m$ is usually related to the domain spacing $\Lambda_m$:

$$\Lambda_m = 2\pi/q_m \tag{4}$$

In the late stage of SD where the amplitude of the composition fluctuations reaches an equilibrium value locally, if the phase-separating structure grows with self-similarity, the relation between $\alpha$ and $\beta$ is usually given by[19−21]

$$\beta = 3\alpha \tag{5}$$

The values $q_m$ and $I_m$ for the 60/40 mixture at 56 and 57 °C were obtained as a function of $t$ from the time change in the LS profiles. Furthermore, for a comparison, we obtained the time change in $q_m$ and $I_m$ for the 50/50 mixture at 60 °C, which is expected to separate into two phases with nearly equal phase volumes from the phase diagram (see Figure 2), and therefore the phase-separating morphology is expected to have percolating structures until a very late stage of phase separation (at least up to 4000 min).

Double-logarithmic plots of (a) $q_m$ vs $t$ and (b) $I_m$ vs $t$ for the 60/40 mixture and for the 50/50 mixture are shown in Figure 3. The $q_m$ and $I_m$ for the 50/50 mixture at 60 °C evolve with time according to the power law with its exponents of $\alpha \approx 1$ and $\beta \approx 3$, respectively, at the long time $t > 700$ min. The value $q_m$ at $t \geq 4000$ min becomes so small that the peak position $q_m$ exists outside the $q$-window of our observation (∼0.000 45 $nm^{-1}$) with our LS apparatus. In such a case, we estimated the value $q_m$ from the position of spinodal ring projected on a screen.

According to Siggia[22] and Kawasaki and Ohta,[23] the percolating structures are predicted to grow with an exponent of $\alpha = 1$ in the time region where hydrodynamic interactions are dominant. As a matter of fact, the phase-separating structures with seemingly percolating morphology are experimentally confirmed to grow with the exponent of $\alpha = 1$ for many binary simple liquids.[24−26] Thus, the phase-separating structures for the 50/50 polymer mixture at 60 °C are considered to have percolated structures and to grow with hydrodynamic interactions.

Next let us consider the time change in the $q_m$ and $I_m$ for the 60/40 mixture at 56 °C. Their behaviors are

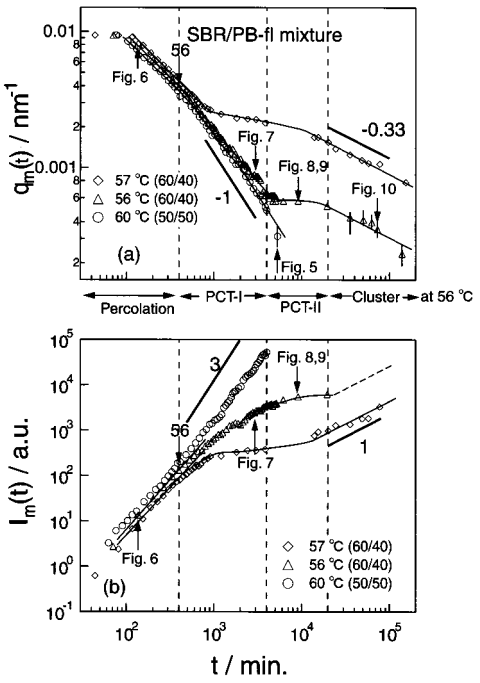


**Figure 3.** Double-logarithmic plots of (a) $q_m$ vs $t$ and (b) $I_m$ vs $t$ for the 50/50 and 60/40 mixtures. This figure also shows percolation, PCT-I, PCT-II, and cluster regimes for the 60/40 mixture at 56 and 57 °C as well as the conditions (time, $q_m$ and $I_m$) where Figures 5−10 are taken. The solid lines through data points and the broken line for $I_m$ for the 60/40 mixture at 56 °C at $t \geq 20\,000$ min are for visual guides.

different from that for the 50/50 mixture at 60 °C. At 56 °C, $q_m$ evolves with an exponent of $\alpha = 0.7-0.8$ and $I_m$ grows with an exponent of $\beta \approx 2.2$ at $130 \leq t \leq 400$ min (the straight line). Afterward, the rate of the decrease in $q_m$ and the rate of the increase in $I_m$ are gradually changed, and hence the time changes in $q_m$ and $I_m$ deviate from the respective straight lines with the exponent of $\alpha = 0.7-0.8$ and that of $\beta \approx 2.2$. The onset of deviation from the straight line is pointed by the arrows numbered 56 in Figure 3a,b. At $4000 \leq t \leq 20\,000$ min, the growth of $q_m$ and the growth of $I_m$ become very slow, and they appeared as if they stopped. At 57 °C a similar behavior as described above is observed, except for the shift of the characteristic time ranges; $130 \leq t \leq 400$ min and $4000 \leq t \leq 20\,000$ min correspond to $120 \leq t \leq 300$ min and $700 \leq t \leq 15\,000$ min, respectively.

As discussed in some earlier articles,[6,8,9,11] this slowing down of phase separation kinetics is considered to be caused by the change in phase-separating morphology from percolated structures to a cluster of droplets, i.e., percolation-to-cluster transition (PCT). Quench depth dependencies on the growth rate of the phase-separating domains in the slowing regime and the onset time of the slowing down of domain growth in this study also show the same trend as those observed in other studies concerning PCT.[6,8,9] As will be discussed in the following section, the analysis of scaled structure factor will support the fact that PCT occurred at the time when the slowing down of increase in $I_m$ starts to take place. In the long time limit ($t \geq 20\,000$ min), $q_m$ at 56 °C grows according to the power law of $\alpha \approx 0.33$.[27] Similarly, at 57 °C in the long time limit ($t \geq 15\,000$ min), $q_m$ and $I_m$ grow with $t$ according to the power law of $\alpha \approx 0.33$ and $\beta \approx 1$, respectively.

In the previous paper,[8] we reported that the phase separation dynamics involving PCT is divided into three

regimes: (i) the percolation regime, (ii) the PCT regime, and (iii) the cluster regime.[8] In the percolation regime, the phase separation dynamics showed the growth law of percolating domains with hydrodynamic interactions (with the exponents of $\alpha \approx 0.9$ and $\beta \approx 2.7$). In the PCT regime, crossover of phase separation dynamics from the percolation regime to the cluster regime was observed. In this regime, after PCT occurred, the phase separation kinetics gradually slowed, and afterward it became very slow as if the domain growth was apparently pinned. In the cluster regime which is the long time limit, the time evolution of phase-separating domains obeyed the growth law of a cluster of droplets.

In this work, the phase separation behavior for the 60/40 mixture at $t \leq 400$ min at 56 °C and that at $t \leq 300$ min at 57 °C are considered to correspond to that in the percolation regime. However, the values of $\alpha$ ($\approx$0.6−0.8) and $\beta$ ($\approx$1.9−2.2) are slightly smaller than those predicted from growth law of percolating domains with hydrodynamic interactions ($\alpha = 1$ and $\beta = 3$). These small values of $\alpha$ and $\beta$ may be caused by the fact that the hydrodynamic effects were not yet completely dominant in this time region. Koga et al. reported that the effects of hydrodynamic interactions on the phase separation dynamics gradually become effective with time and completely dominate the domain growth mechanism in the *late stage* of phase separation.[28,29] For mixtures of polymers with high molecular weight, hydrodynamic interactions become important in the *very late stage* of phase separation.[30] Hence, we think that in the phase separation process at 56 °C the PCT occurred before the effects of hydrodynamic interactions completely dominate the domain growth mechanism. For example, for 50/50 mixture, we should note that $q_m$ obeyed the power law of $\alpha \approx 1$ at much later time than 400 min, i.e., $700 \leq t \leq 2000$ min.

The phase separation behaviors at $400 \leq t \leq 20\,000$ min at 56 °C and that at $300 \leq t \leq 15\,000$ min at 57 °C correspond to that in the PCT regime. Here we further divide this regime into two regimes: (i) the PCT-I regime ($400 \leq t \leq 4000$ min at 56 °C and $300 \leq t \leq 700$ min at 57 °C) and (ii) the PCT-II regime ($4000 \leq t \leq 20\,000$ min at 56 °C and $700 \leq t \leq 15\,000$ min at 57 °C). In the PCT-I regime, while the growth rate of $q_m$ was almost as fast as that in percolation regime, the growth rate of $I_m$ gradually became slow with time. In the PCT-II regime, the growth of both $q_m$ and $I_m$ was very slow. The difference between phase separation dynamics in the PCT-I regime and that in the PCT-II regime is speculated as follows. In the PCT-I regime, after the onset of PCT occurred, the domains still remained percolated over a large length scale, though they lost a macroscopic percolation. Since these percolated domains are expected to grow in almost the same mechanism as that in infinitely percolating domains with hydrodynamic interactions, the growth rate with respect to $q_m$ is fast. However, the growth rate of $I_m$ decreases with time due to PCT. The reason for the decrease in the growth rate of $I_m$ after the onset of PCT was reported in the previous papers.[8,9]

In the PCT-II regime, there may not exist any domains percolating in the long range. In this regime, the domains percolating in a very short range or the locally interconnected domains may be transformed into droplets in order to reduce the interfacial free energy, and afterward it may take some time for the droplets to grow via diffusion and coalescence processes. In this process, the phase-separating domains are expected to hardly grow. Hence, the time evolutions of both $q_m$ and $I_m$ in the PCT-II regime are considered to be very slow.

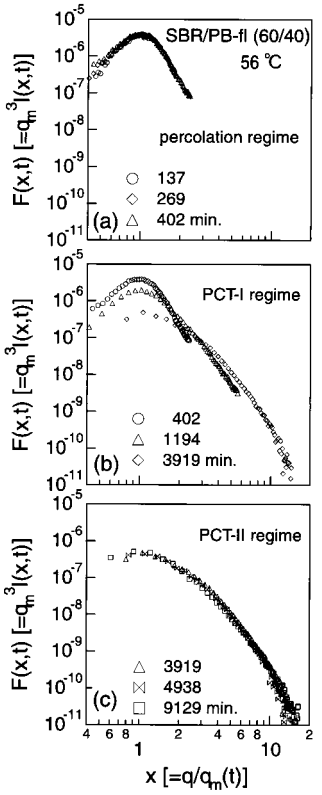


**Figure 4.** Time change in scaled structure factor for the 60/40 mixture at 56 °C, in the (a) percolation regime, (b) PCT-I regime, and (c) PCT-II regime.

The phase separation behaviors at $t \geq 20\,000$ min at 56 °C and $t \geq 15\,000$ min at 57 °C are considered to correspond to that in the cluster regime. The phase separating droplets grow according to the Lifsitz−Slyozov−Wagner law[31,32] or diffusion coalescence of droplets with hydrodynamic interactions ($\alpha \approx 0.33$ and $\beta \approx 1$).[19]

Thus, the phase separation dynamics at 56 °C for 60/40 mixture can be classified into four regimes: (i) the percolation regime, (ii) the PCT-I regime, (iii) the PCT-II regime, and (iv) the cluster regime. Each characteristic time range shifts to a shorter time scale with increasing temperature of phase separation.

**C. Scaled Structure Factor Analysis.** The scaled structure factor $F(x,t)$ is defined by

$$F(x,t) \equiv q_m(t)^3 I(q,t) = K\langle \eta(t)^2 \rangle S(x,t) \qquad (6)$$

where $\langle \eta(t)^2 \rangle$ is the mean-squared fluctuations of refractive index and $S(x,t)$ is a universal scaling function characterizing the form of the phase-separating domains, and $K$ is a proportionality constant. In the late stage of spinodal decomposition (SD) for critical mixtures of small molecules and for those of polymers whose components have nearly equal molecular weight and viscosity, it has been found that $F(x,t)$ becomes a universal function independent of $t$.[30,33,34]

In Figure 4, we show a time change in $F(x,t)$ in each regime at 56 °C for the 60/40 mixture. Since we could not measure the LS intensity around the peak position in the cluster regime ($t \geq 20\,000$ min), because the position existed outside of the $q$-window of our LS

apparatus, there is no $F(x,t)$ data in this regime. The $F(x,t)$ from $t = 137$ to $t = 402$ min in the percolation regime becomes a universal function against $t$ as seen in the late stage of SD for critical mixtures of small molecules and for those of polymers whose components have nearly equal molecular weight and viscosity. This behavior means that, as seen from eq 6, $\langle \eta(t)^2 \rangle$ attains the equilibrium value predicted from the phase diagram, and $S(x,t)$ does not change with time, i.e., the phase-separating structures grow with "dynamical self-similarity".[19] At $402 \leq t \leq 3919$ min in the PCT-I regime, $F(x,t)$ becomes broader with $t$ (Figure 4b). As reported in the previous papers,[8,9] this behavior is caused by PCT. Thus, the scaled structure factor analysis indicates that PCT at 56 °C starts to occur at $t \approx 400$ min, consistent with the results found in the time change in $q_m$ and $I_m$ shown in Figure 3. In the PCT-II regime, while $F(x,t)$ is independent of $t$ at $x \approx 1$, at a high $x$ range ($\geq 2.5$) it is slightly nonuniversal with $t$ (Figure 4c). The former behavior reflects that $q_m$ and $I_m$ in this regime hardly change with $t$. As discussed in the previous section from time evolution of $q_m$ and $I_m$, we speculated that in the PCT-II regime locally percolated phase-separating domains induced by PCT may change into round droplets with time. Such a change in the interface of phase-separating domains may affect the scattering profile at the high $x$ range, which is consistent with the behavior of $F(x,t)$ in Figure 4c.

Thus, the behavior of $F(x,t)$ in each regime is consistent with our speculation based on the time change in $q_m$ and $I_m$ in Figure 3.

**D. Real-Space Observation of Phase-Separating Domains by TEM and LSCM.** Figure 5 shows LSCM pictures of phase-separating domains in the (a) $y,z$-plane, (b) $x,y$-plane, and (c) $x,z$-plane taken at $t = 5297$ min after the onset of the phase separation for the 50/50 mixture at 60 °C (see Figure 1 about the scanning geometry). The bright phase is the one which emits stronger fluorescent light than the dark phase and hence corresponds to the PB-fl-rich phase, while the dark phase corresponds to the SBR-rich phase. The phase-separating domains observed in the $x,y$-plane are bicontinuous or percolating (Figure 5b). Moreover, as shown in parts a and c of Figure 5, the $y,z$ and $x,z$ cross-sectional images produced by stacking 50 LSCM slices along the $z$-direction, respectively, show clearly that the phase-separating domains are percolating, too.

Note, for example, that the bright domain marked by the arrow with number (1) in Figure 5b appears to be isolated in the dark matrix phase. However, this domain is seen to be interconnected with the PB-fl-rich domain along the depth direction ($z$-axis) as clearly shown in the $y,z$ *cross*-sectional image in Figure 5a {see the arrow with number (1)}. Note also that the dark domain marked by the arrow with number (2) surrounded by the bright domain in Figure 5c is continuously connected with the dark phase in the $x,y$-plane as shown by the arrow marked by number (2) in Figure 5b. Thus, the phase-separating structures are shown to be three-dimensionally percolating, which is consistent with our prediction from the LS result. The spacing of percolating domains $\Lambda_m$ observed from the LSCM picture is ca. 20−30 $\mu$m, which is consistent with that estimated from $q_m$ by using eq 4 ($\Lambda_m = 21$ $\mu$m).

Next, we investigated the phase-separating morphology in each regime defined in section III.B for the 60/40 mixture at 56 °C by means of TEM and LSCM.

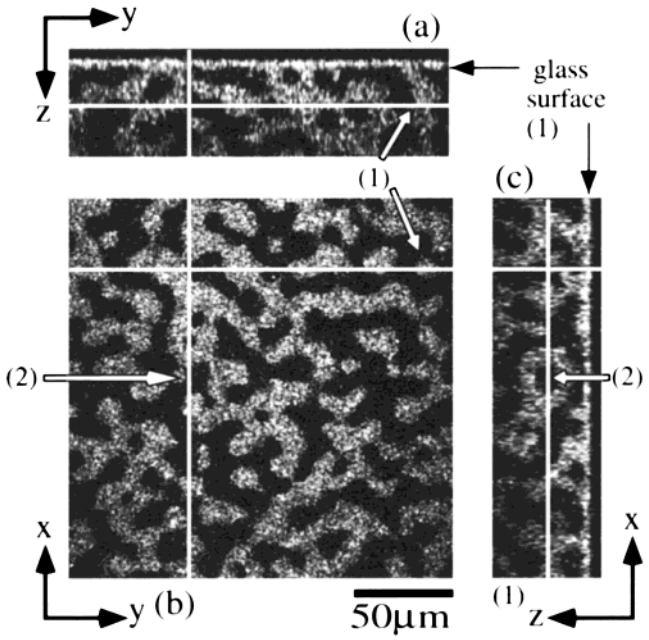


**Figure 5.** LSCM images of phase-separating structures for the 50/50 mixture in the (a) $y,z$-plane, (b) $x,y$-plane, and (c) $x,z$-plane at 5297 min after onset of the phase separation at 60 °C. The LSCM image in the $x,y$-plane was observed by directly detecting the fluorescent light emitted from the focal plane. The LSCM images in the $y,z$-plane and in the $x,z$-plane were produced from cross sections of 50 LSCM slices taken by moving the focal plane along the $z$-direction at every 1 $\mu$m interval, in respective planes, as shown in Figure 1. White lines in the figures show the position where cross-sectional images are taken, as illustrated in Figure 1. For example, (a) corresponds to the image cross-sectioned along the horizontal white line in (b). (c) corresponds to the image cross-sectioned along the vertical white line in (b). (b) corresponds to the image cross-sectioned along the horizontal white line in (a) or the vertical white line in (c) (22.5 $\mu$m below the glass surface).

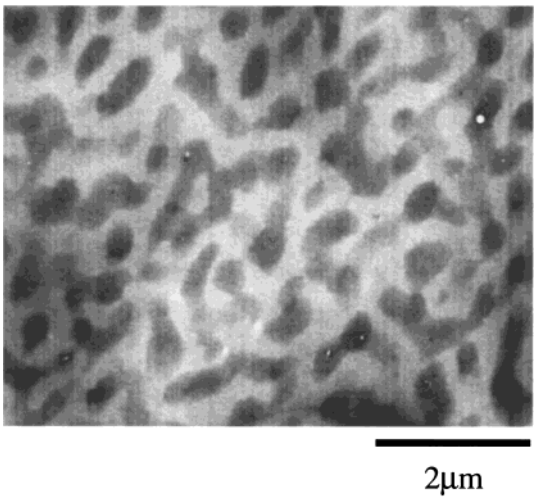


**Figure 6.** A TEM image of phase-separating domains obtained with the ultrathin section (~50 nm thick) stained with osmium tetraoxide for the 60/40 mixture annealed at 56 °C for 125 min.

Figure 6 shows a TEM picture of the phase-separating structures obtained for the specimen annealed for 125 min at 56 °C. The mixture is in the percolation regime at this phase separation time. The phase-separating structures ($\Lambda_m \approx 0.8$ $\mu$m) in this time range are so small that we cannot observe them by means of LSCM. In the TEM picture, dark phases (or domains) are PB-fl-rich phases, which are stained with $OsO_4$ more heavily than

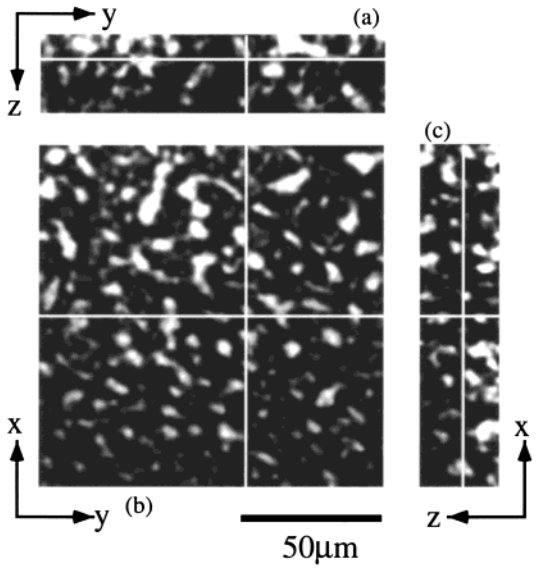


**Figure 7.** LSCM images of phase-separating structures in the (a) *y*,*z*-plane, (b) *x*,*y*-plane, and (c) *x*,*z*-plane for the 60/40 mixture at 3004 min after onset of the phase separation at 56 °C. The LSCM images in this figure were obtained in the same manner as those in Figure 5, except that we used 30 LSCM slices instead of 50 slices in order to obtain the image in the *y*,*z*-plane and that in the *x*,*z*-plane.

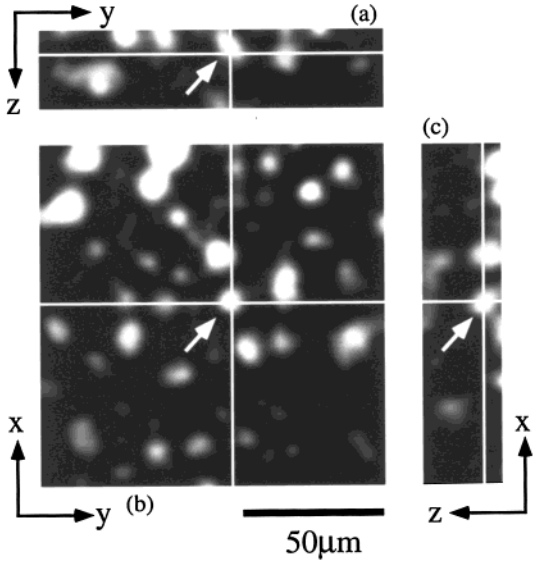


**Figure 8.** LSCM images of phase-separating structures in the (a) *y*,*z*-plane, (b) *x*,*y*-plane, and (c) *x*,*z*-plane for the 60/40 mixture at 8826 min after onset of the phase separation at 56 °C. The LSCM images in this figure were obtained in the same manner as those in Figure 7.

the SBR-rich phases. The TEM picture shows that dark domains are interconnected and percolated in the bright matrix domain over all the area observed in the figure, generating dark-to-gray-to-bright (contrast) variation depending on their three-dimensional spatial arrangements in the ultrathin section. Although some of the dark domains look like isolated domains, we believe that this is due to the fact that the ultrathin section used in the TEM observation (∼50 nm thickness) is much smaller than the periodicity of the phase-separating domains ($\Lambda_m \approx 0.8$ $\mu$m). Namely, in such a case, interconnections among domains are sometimes cut off, and therefore the interconnected domains are apparently isolated. We will demonstrate this fact by showing some LSCM images taken along the *z*-direction as will be shown in Figure 9 later. Thus, the dark domains are expected to be completely percolating in the percolation regime.

In Figure 7 we present the LSCM images of the phase-separating structures in the (a) *y*,*z*-plane, (b) *x*,*y*-plane, and (c) *x*,*z*-plane for the 60/40 mixture at 56 °C at $t = 3004$ min after the onset of phase separation (the PCT-I regime). The LSCM images of the phase-separating domains in the *y*,*z*-plane and in the *x*,*z*-plane were obtained by stacking 30 LSCM slices with 1 $\mu$m distance along the *z*-direction (see Figure 1). The interdomain distance is still small (∼7 $\mu$m), consistent with the result shown in Figure 3. Many of the bright PB-fl-rich domains in the *x*,*y*-plane are not macroscopically percolating but are only locally interconnected in the dark SBR-rich matrix phase. The images in the *y*,*z*-plane and in the *x*,*z*-plane also show that the bright domains are interconnected over only a small length scale. Here, it is very important to pay attention to the length scale of the interconnections: some interconnections among domains in the cross-sectional image are probably cut off, if focal depth is much smaller than the domain size, even though they may exist in the direction perpendicular to the cross-sectional image. Therefore, the length scale of interconnection among domains in the cross-sectional image tends to be underestimated, which will be demonstrated in Figure 9 later. In any case, in this time range, PCT is considered to have already started, consistent with the LS result.

Figure 8 presents the LSCM images of the phase-separating structures in the (a) *y*,*z*-plane, (b) *x*,*y*-plane, and (c) *x*,*z*-plane for the 60/40 mixture annealed at 56 °C for 8826 min (the PCT-II regime). The image in each plane was obtained in the same manner as that in Figure 7. Most of the bright domains have a rather round shape relative to those shown in Figure 7. Moreover, it is obvious that there are almost no connected domains in each image. Note, for example, that the bright domain marked by an arrow in Figure 8b is surrounded by the dark domain and has quite round shape. This situation is also the case in the *y*,*z*-section in Figure 8a and in the *x*,*z*-section in Figure 8c (see the bright domain marked by the arrow in the respective figures). Moreover, the size of the phase-separating domains (∼15 $\mu$m) is larger than that in Figure 7, indicating that growth of phase-separating structures proceeded after the onset of PCT. Thus, a comparison of the LSCM image in Figure 8 with that in Figure 7 reveals that, after the onset of PCT, the phase-separating domains grew for some period to break up into cluster of the fragments of the locally percolated domains and the fragments were then transformed into domains with a round shape. It is also observed that the number of the domains decrease with time as usual for ordering in conserved order parameter systems.

Here we would like to emphasize that a single LSCM slice image should be cautiously interpreted in visualizing the three-dimensional (3D) phase-separated domains in some cases. As shown in Figure 9, representing the same sample condition as that in Figure 8, if we carefully look at a series of the LSCM sliced images taken from the same area of the sample just by moving the focal plane at 2 $\mu$m intervals along the *z*-direction, we notice that a single LSCM sliced image may sometimes mislead us as to interpretation of its 3D morphology. For example, let us concentrate on three domains surrounded by white circles on the right-hand side of

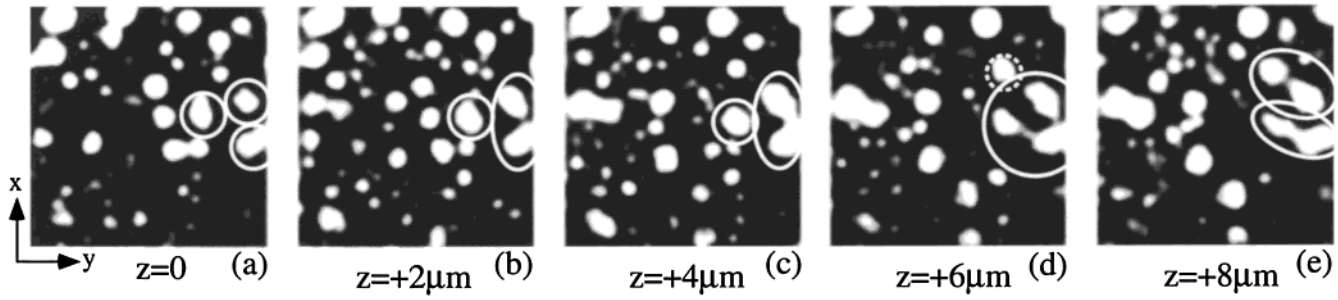


**Figure 9.** LSCM images of phase-separating structures for the 60/40 mixture at 8826 min after the onset of phase separation at 56 °C. A series of the sliced images in the *x*,*y*-plane were taken on the same area of the sample by shifting only the focal depth along *z*; at (a) $z = 0$, (b) $z = +2$, (c) $z = +4$, (d) $z = +6$, and (e) $z = +8$ ($\mu$m) relative to the image (a).

the image in the *x*,*y*-plane at a given *z* in Figure 9a (we define the position of *z* as $z = 0$). Apparently, these PB-fl-rich domains are not connected and are separated in the dark SBR-rich phase. However, if we observe the LSCM slice in the *x*,*y*-plane at $z = +2$ $\mu$m or that at $z = +4$ $\mu$m (see Figure 9b or Figure 9c), the two of them are found to be interconnected. Furthermore, if we observe a single LSCM slice in the *x*,*y*-image at $z = +6$ $\mu$m (see Figure 9d), then all of them are found to be interconnected. Moreover, in Figure 9d the domain surrounded by a white dotted circle and that surrounded by a white circle are apparently separated. However, these domains are also shown to be interconnected from the image at $z = +8$ $\mu$m (see Figure 9e). Thus, to judge whether some domains are interconnected or not, it is necessary to take a series of sliced images along the *z*-direction. In other words, we need to have three-dimensional information on the phase-separating domains. The three-dimensional image of the phase-separating structures in each regime will be presented and discussed in the following section.

We show the LSCM images in the (a) *y*,*z*-plane, (b) *x*,*y*-plane, and (c) *x*,*z*-plane for the 60/40 mixture taken at 73 136 min after the onset of phase separation at 56 °C in Figure 10 (cluster regime). The phase-separating domains in each plane have fully round shape and are separated each other in the dark matrix rich in SBR. For example, the domain situated in the middle of Figure 10b appears round in *y*,*z*-plane in Figure 10a and in the *x*,*z*-plane in Figure 10c (see the domain marked by the circle). Thus, the phase-separating domains are considered to be droplets in the cluster regime. This result is also consistent with the LS result.

**E. Three-Dimensional Image of the Phase-Separating Structures in Each Regime.** We constructed a three-dimensional (3D) image of the phase-separating structures by computationally stacking 30 sliced images which are obtained by moving the focal plane (*x*,*y*-plane) along the *z*-direction at 1 $\mu$m intervals.[35] We present the 3D images of the phase-separating structures for the 60/40 mixture at (a) 3004 min (the PCT-I regime), (b) 8826 min (the PCT-II regime), and (c) 73 136 min (the cluster regime) after onset of the phase separation at 56 °C in Figure 11. As described in the previous section, the phase-separating domains in the percolation regime were too small to be observed with LSCM. Therefore, the corresponding 3D image is not shown in Figure 11.

Though the phase-separating domains in Figure 11a are not infinitely percolating, most of the domains are percolating over a large length scale. Note that the length scale of the percolation observed by the 3D image is much longer than that observed in the cross-sectional

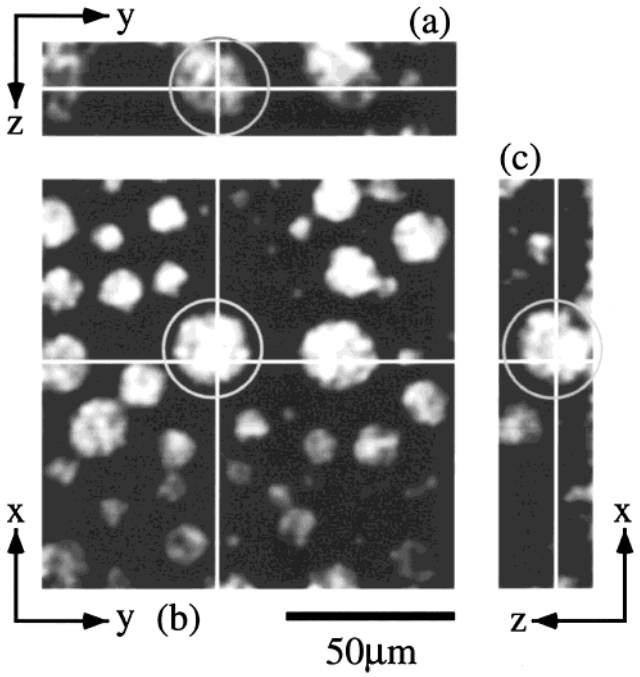


**Figure 10.** LSCM images of phase-separating structures in the (a) *y*,*z*-plane, (b) *x*,*y*-plane, and (c) *x*,*z*-plane for the 60/40 mixture at 73 136 min after the onset of phase separation at 56 °C. The LSCM images in this figure were obtained in the same manner as those in Figure 7.

image in Figure 7. Thus, in the PCT-I regime, the phase-separating domains still keep traces of percolating structures although the PCT has already started. Hence, their growth is predicted to be similar to the growth of percolating structures. For this reason, the time evolution of $q_m$ in the PCT-I regime is considered to be as fast as that in percolation regime, as discussed in section III.B.

In Figure 11b, the bright domains appear to be only locally interconnected in comparison with that in Figure 11a. Therefore, they cannot grow in the same manner as that in the PCT-I regime. These locally interconnected domains are expected to be further transformed into round droplets with elapse of time in order to reduce the interface area and the interfacial free energy. This process hardly affects time change in $q_m$, giving the exponent $\alpha \approx 0$, also consistent with the LS result.

As shown in Figure 11c, many of the phase-separating domains in cluster regime are droplets with round shape. In these domains, a trace of the percolating structures scarcely remains. However, some domains appear to be interconnected droplets or dumbbells. The reason for this is speculated as follows: the dumbbells

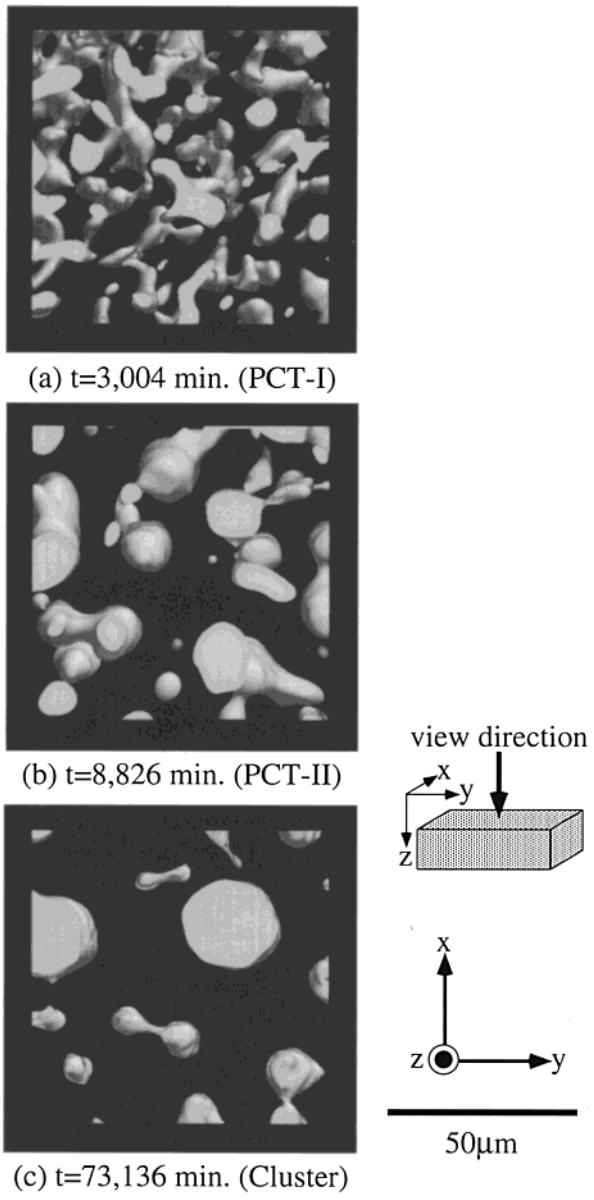


**Figure 11.** 3D images of the phase-separating structures in each regime except for the percolation regime for the 60/40 mixture: (a) 3004 min (PCT-I regime), (b) 8826 min (PCT-II regime), and (c) 73 136 min (cluster regime) after the onset of phase separation at 56 °C. The method of construction of these 3D images is described in ref 35. The direction of view of each image is indicated in the figure. The 3D images were constructed from 30 slices taken at distance of 1 $\mu$m intervals along $z$-direction.

may reflect a snapshot of the process in which the coalesced droplets or a part of anisotropic domains disconnected from other domains are transformed into round droplets.

In summary, we succeeded in constructing the 3D images of the phase-separating structures of a binary mixture of polymers involving PCT. The 3D LSCM images clarified four regimes of the phase separation processes and the characteristic 3D structures in each regime.

## IV. Conclusion

We investigated the dynamics of phase separation and time evolution of morphology for an SBR/PB-fl mixture involving percolation-to-cluster transition (PCT) by means of the combined Fourier-space and real-space observations with laser scanning confocal microscopy (LSCM) and light scattering (LS). By using the LSCM technique, we successfully clarified time evolution of the three-dimensional (3D) images of the phase-separating structures for the mixture undergoing PCT in the phase separation process. Furthermore, this study demonstrated that the LSCM technique, which can obtain 3D information on the phase separating domains, was very powerful in the studies of the phase separation involving the PCT. The phase separation process involving the PCT can be classified into four regimes by LS. The 3D image of the phase-separating domains in each regime was in good agreement with the LS analysis.

**Acknowledgment.** We acknowledge Mr. Yoshihito Tanaka for help with the TEM observation.

## References and Notes

(1) Wilson, T. *Confocal Microscopy*; Academic Press: London, 1990.
(2) Jinnai, H.; Nishikawa, Y.; Koga, T.; Hashimoto, T. *Macromolecules* **1995**, *28*, 4782.
(3) Jinnai, H.; Nishikawa, Y.; Koga, T.; Hashimoto, T. In *Interface Aspects of Multicomponent Polymer Materials*; Lohse, D. J., Russel, T., Sperling, L. H., Eds.; Plenum Press: New York, 1997.
(4) Jinnai, H.; Koga, T.; Nishikawa, T.; Hashimoto, T.; Hyde, S. T. *Phys. Rev. Lett.* **1997**, *78*, 2248.
(5) Hashimoto, T.; Koga, T.; Jinnai, H.; Nishikawa, T. *Nuovo Cimento* **1998**, *20*, 1947.
(6) Hashimoto, T.; Takenaka, M.; Izumitani, T. *J. Chem. Phys.* **1992**, *97*, 679.
(7) Takenaka, M.; Izumitani, T.; Hashimoto, T. *J. Chem. Phys.* **1993**, *98*, 3528.
(8) Takeno, H.; Hashimoto, T. *J. Chem. Phys.* **1997**, *107*, 1634.
(9) Takeno, H.; Nakamura, E.; Hashimoto, T. *J. Chem. Phys.* **1999**, *110*, 3612.
(10) Crist, B. *Macromolecules* **1996**, *29*, 7276.
(11) Läuger, J.; Lay, R.; Gronski, W. *J. Chem. Phys.* **1994**, *101*, 7181.
(12) Kotnis, M. A.; Muthukumar, M. *Macromolecules* **1992**, *25*, 1716.
(13) Brown, G.; Chakrabarti, A. *J. Chem. Phys.* **1993**, *98*, 2451.
(14) Castellano, C.; Glotzer, S. *J. Chem. Phys.* **1995**, *103*, 9363.
(15) Hashimoto, T.; Izumitani, T.; Takenaka, M. *Macromolecules* **1989**, *22*, 2293.
(16) Nishikawa, Y.; Jinnai, H.; Koga, T.; Hashimoto, T.; Hyde, S. T. *Langmuir* **1998**, *14*, 1242.
(17) Ribbe, A. E.; Bodycomb, J.; Hashimoto, T. *Macromolecules* **1999**, *32*, 3154.
(18) See for example: Takeno, H.; Hashimoto, T. *J. Chem. Phys.* **1998**, *108*, 1225.
(19) Binder, K.; Stauffer, D. *Phys. Rev. Lett.* **1974**, *33*, 1006.
(20) Nose, T. *Phase Transitions* **1987**, *8*, 245.
(21) Hashimoto, T. *Phase Transitions* **1988**, *12*, 47.
(22) Siggia, E. D. *Phys. Rev. A* **1979**, *20*, 595.
(23) Kawasaki, K.; Ohta, T. *Physica A* **1983**, *118*, 175.
(24) Wong, N. C.; Knobler, C. *J. Chem. Phys.* **1978**, *69*, 725.
(25) Wong, N. C.; Knobler, C. M. *Phys. Rev. A* **1981**, *24*, 3205.
(26) Chou, Y. C.; Goldburg, W. I. *Phys. Rev. A* **1979**, *20*, 2105.
(27) Since $q_m$ for the 60/40 mixture at 56 °C at $t \geq 20{,}000$ min exists outside the $q$-window of observation with our LS apparatus, we estimated the $q_m$ from the position of the spinodal ring projected on a screen. Therefore, in this time region we could not measure $I_m$.
(28) Koga, T.; Kawasaki, K. *Phys. Rev. A* **1991**, *44*, 817.
(29) Koga, T.; Kawasaki, K.; Takenaka, M.; Hashimoto, T. *Physica A* **1993**, *198*, 473.
(30) Takenaka, M.; Izumitani, T.; Hashimoto, T. *J. Chem. Phys.* **1992**, *97*, 6855.
(31) Lifshitz, I. M.; Slyozov, V. V. *J. Phys. Chem. Solids* **1961**, *19*, 35.
(32) Wagner, C. Z. *Z. Elektrochem.* **1961**, *65*, 581.
(33) Hashimoto, T.; Itakura, M.; Hasegawa, H. *J. Chem. Phys.* **1986**, *85*, 6118.
(34) Wiltzius, P.; Bates, F. S.; Heffner, W. R. *Phys. Rev. Lett.* **1988**, *60*, 1538.

(35) We constructed the 3D images comprised of a series of 30 sliced 2D images by using the volume rendering program "T3D for Machintosh" by Fortner Research LLC. Before constructing the 3D images, we binarized the series of sliced 2D images in the following way: First we enhanced contrast of the images by modifying the overall dynamic range of intensity level of the images. We, then, applied the Gaussian filter to the images to remove the noise. The size of the convolution kernel was determined by trial and error to give a best result. After the enhancement and the filteration, we obtained bimodal intensity distribution of the images. Finally, we binarized the images with the threshold set in the middle of two modes.

MA001316U